ISSN (Print) 1226-1750
ISSN (Online) 2233-6656
Journal of Magnetics 23(2), 192-195 (2018) https://doi.org/10.4283/JMAG.2018.23.2.192

Surface Coil with an Inductively Coupled Wireless Surface and Volume Coil for Improving the Magnetic Field Sensitivity at 400-MHz MRI

Jeung-Hoon Seo[1], Jae Jun Lee[2], and Kyoung-Nam Kim[1]*

[1]*Neuroscience Research Institute, Gachon University, Incheon 21565, Korea*
[2]*Laboratory Animal Center, KBIO Osong Medical Innovation Foundation, Osong, Cheongju-si, Chungbuk 28160, Korea*

(Received 7 March 2018, Received in final form 22 June 2018, Accepted 22 June 2018)

This work presents the use of combinations between a wireless radio-frequency surface coil and a wireless 16-leg birdcage coil that are inductively coupled to improve the magnetic field sensitivity and uniformity. A single surface loop coil operating as transmission/reception (Tx/Rx) coil was designed for mouse head imaging at a magnetic field strength of 9.4-T. Numerical analyses using finite-difference time-domain were performed to compute the sensitivity and homogeneity of magnetic and electric flux density fields for each of the coil combinations. Maximum field values and standard deviation were used as statistical parameters to compare the sensitivity and homogeneity of the fields produced by the Tx/Rx surface coil for each case, when the wireless inductively coupled coils were used. The electromagnetic analyses were applied to a cylindrical oil-based phantom and a mouse model. The proposed combinations of the surface coil with the inductively coupled wireless surface and wireless volume coils offer an enhanced magnetic-flux sensitivity and RF excitation field distribution at 9.4-T. The modifications to the surface coil geometry by adding the inductively coupled radio-frequency coil combinations could be applied to the generally used transmit/receive surface coils and extended to parallel radio-frequency transmission array at ultra-high-field magnetic resonance imaging.

Keywords : Magnetic Resonance Imaging (MRI), Radiofrequency (RF) coil, Inductively coupled coil, 9.4-T

1. Introduction

The magnetic resonance imaging (MRI) is a diagnostic medical imaging technique based on nuclear resonance spectrometer, which uses the physical phenomena between an atomic nucleus in an external magnetic ($|B_0|$)-field and an electromagnetic (EM) wave having a specific resonance frequency. As the strength of $|B_0|$-field increases, high-quality anatomical images are obtained. Because signal-to-noise ratio (SNR) increases linearly with the $|B_0|$-field strength, more than 50 institutions with 7.0-T, a few 9.4-T and 10.5-T, and 11.7-T for human brain studies [1] and 21.1-T for animal studies. A higher image resolution helps investigate detailed anatomic information and provides better localization. However, the application of short radiofrequency (RF) waves, during by high-frequency operations, to biological tissues is still a challenge [2]; the main reason being that the RF wavelength within a tissue depends on the tissue's electrical properties such as conductivity (σ) and relative permittivity (ε_r). σ increases and ε_r decreases with increasing resonance frequency of the $|B_0|$-field. A short RF wavelength can exhibit a complicated wave behavior inside the biological tissue, resulting in degraded MR image quality due to inhomogeneous magnetic flux density ($|B_1|$)-field distribution in high-frequency operations. Nevertheless, a single-channel volumetric coil or a surface coil can be utilized and adapted with high frequency despite the inhomogeneous distribution of $|B_1|$-field [3]. In such cases, by using the volume, the amount of noise generated from the test subject is high for a large subject. Therefore, the SNR is relatively lower as compared to a small-size surface coil [4]. On the other hand, the surface coil is mainly used for MR image acquisition of a local region, despite inhomogeneous $|B_1|$-field distribution. The geometry of the surface coil for a local imaging region can be rectangular, circular, elliptical, polygonal, or octagonal, depending on the shape of the target imaging region. The mode of the surface coil is generally transmission/reception (Tx/Rx) or Rx-only [5]. The imaging area of the surface coil is generally designed

*Corresponding author: Tel: +82-32-460-9015
Fax: +82-32-460-8230, e-mail: jeunghoon.seo@gmail.com

to be half the diameter of the coil, and the imaging region depends on the depth pulse sequence, which is the applied RF energy on the test subject [6]. Although the surface coil has the advantage of a higher $|B_1|$-field sensitivity in the region adjacent to the coil, the signal intensity of $|B_1|$-field rapidly decreases away from the coil. To overcome this problem, addition of a high-permittivity material (HPM) attachment or an inductively coupled wireless coil (*w*-ICWC) is suggested with a small field of view (FOV) to increase the overall $|B_1|$-field distribution [7, 8].

In this paper, the inductively coupled wireless volume coil (*w*-ICWVC) was used to increase the uniformity of $|B_1|$-field in the surface coil and to increase the homogeneity of $|B_1|$-field in an environment with a short-RF-wavelength MRI system. The Tx/Rx surface coil with the *w*-ICWVC was compared to the inductively coupled wireless surface coil (*w*-ICWSC) and the combination of the *w*-ICWVC and *w*-ICWSC. EM calculations were performed to explore the distribution of the $|B_1|$-field and electric ($|E|$)-field, with an oil-based cylindrical phantom and a mouse model.

2. Materials and Methods

To evaluate the performance of the *w*-ICWVC and *w*-ICWSC in the single-channel Tx/Rx coil, finite-difference time-domain (FDTD) was utilized to compute the EM-field by using Sim4Life (Speag, Switzerland) [9]. The voxel size was set to 372 × 372 × 190 Yee cells along the x-, y-, and z-directions for an oil-based cylindrical phantom, and 522 × 372 × 340 Yee cells for a mouse model (Male PIM1 mouse from IT'IS Foundation (Information Technologies in Society), Switzerland) as shown in Fig. 1. The dimensions of the oil-based cylindrical phantom were 30 mm diameter and 100 mm length. The dielectric properties of the oil-based cylindrical phantom included a conductivity of 0 $S \cdot m^{-1}$ and a permittivity of 4, which is similar to that of oil. Each calculating resolution having a 1 mm resolution in the x-, y-, and z-directions. The EM calculations were performed at 400 MHz of 9.4-T and four RF excitation in the single-channel Tx/Rx coil was set as current source of 1 A. The general approach of using the single-channel Tx/Rx surface coil was model as shown in Fig. 1(a). The coil dimensions were 20 mm length and 2 mm breadth, under a perfect electric conductor. The interval between the coil and the oil-based cylindrical phantom was 1 mm, but the interval in the mouse model was 15 mm. Other comparing condition of *w*-ICWSC configuration as shown in Fig. 1(b). In detail, the Tx/Rx surface coil and the *w*-ICWSC were separately

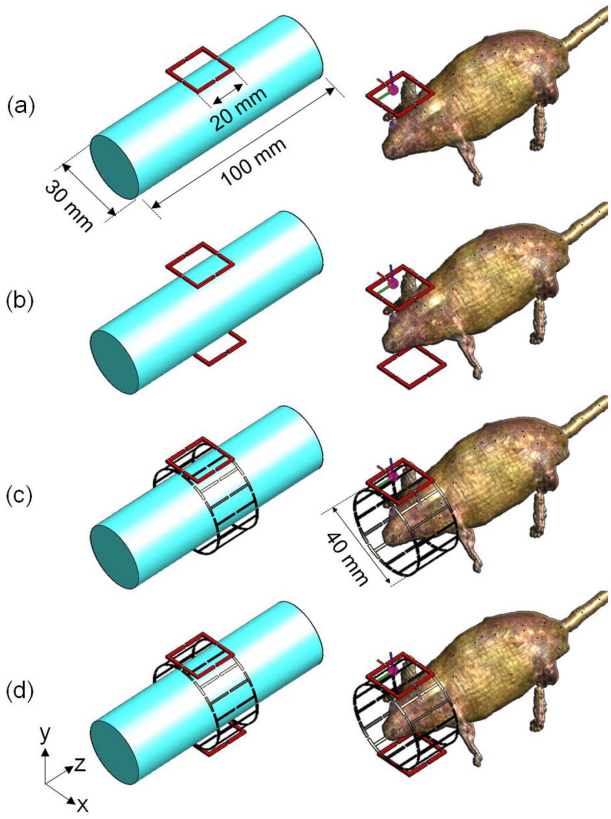

Fig. 1. (Color online) Geometric models of four types coil configurations for the finite-different time-domain (FDTD) calculation using oil-based cylindrical phantom and mouse model: (a) single-channel Tx/Rx surface coil, (b) single-channel Tx/Rx surface coil + *w*-ICWSC, (c) single-channel Tx/Rx surface coil + *w*-ICWVC, (d) single-channel Tx/Rx surface coil + *w*-ICWSC + *w*-ICWVC.

positioned in the oil-based cylindrical phantom and the mouse model. The existence and nonexistence of the EM field shows different behaviors in the coil and the wireless coil. Four distributed capacitors in the *w*-ICWSC were set at 15 pF for a frequency of 400-MHz. The coil configuration of the *w*-ICWVC is shown in Fig. 1(c). The wireless birdcage coil is closely positioned in the single-channel Tx/Rx surface coil. The 16-leg band-pass-filter birdcage coil with 32 RF sources and a sinusoidal current source and a geometric phase distribution was employed. The coil dimensions were 40 mm diameter and 20 mm length. The band-pass-filter birdcage coil was set at 18 pF in the end-ring and 67 pF in the leg region for 9.4-T frequency of 400-MHz. The last coil configuration combined geometries of the *w*-ICWVC and the *w*-ICWVC on the single-channel Tx/Rx surface coil, as shown in Fig. 1(d).

3. Results and Discussion

The $|B_1|$-field involving RF excitation ($|B_1^+|$) distributions for three four coil configurations at 9.4-T of 400-MHz frequency were obtained and compared using FDTD calculations (in units of μT/V) as shown in Fig. 2. The overall high $|B_1|$-field as well $|B_1^+|$-field sensitivity of the *w*-ICWVC and the combined geometry of the *w*-ICWSC and *w*-ICWVC on the single-channel Tx/Rx surface coil were measured on the oil-based cylindrical phantom and a mouse model. Particularly, the performance of $|B_1^+|$-field appeared to be similar to $|B_1|$-field distribution owing to the reciprocal theory [10]. For a more detailed investigation, two evaluating factors–maximum and standard deviation (SD) of the $|B_1|$- and $|B_1^+|$-map–were measured and compared. The measured values between the single-channel Tx/Rx coil and the *w*-ICWSC were similar to the values provided in Table 1. The difference between the maximum and the SD values in the oil-based cylindrical phantom was 0.007 μT and 0.001 μT for $|B_1|$-field. In case of the mouse model, 0.009 μT and 0.016 μT were measured as the difference between the maximum $|B_1|$-field intensity and the SD values, respectively. These results clearly indicate that the performance of the two coils is very similar to each other in terms of $|B_1|$-field sensitivity and homogeneity. However, the *w*-ICWVC showed a relatively higher maximum $|B_1|$-field intensity and a lower SD value for the oil-based cylindrical phantom and mouse model. The measured maximum $|B_1|$-field intensity was 4.052 μT and 3.153 μT for the oil-based cylindrical phantom and the mouse model, respectively. In addition, the SD value of the *w*-ICWVC coil configuration was 0.258 μT and 3.019 μT for the oil-based cylindrical phantom and the mouse model, respectively. The measured maximum $|B_1|$-field intensity of the *w*-ICWVC coil configuration was approximately 2 times higher than the $|B_1|$-field sensitivity, as compared to the coil configurations of the single-channel Tx/Rx coil and the *w*-ICWSC coil. Furthermore, the SD value of the *w*-ICWVC was approximately 3 times lower than the two coils. The results reflect that the *w*-ICWVC coil had higher $|B_1|$-field sensitivity and homogeneity as compared to the two-coil cases. The single-channel Tx/Rx surface coil with the *w*-ICWSC and the *w*-ICWVC coils was compared in the same way. The maximum $|B_1|$-field intensity and SD values were similar to that of the *w*-ICWVC. The differentiation of two evaluating factors was approximately 2 % for the two-coil cases. From these results, it appears that the $|B_1|$-field distribution is more dependent on the *w*-ICWVC rather than the *w*-ICWSC configuration. According to the $|B_1|$-field simulation results, the *w*-ICWVC configuration has higher sensitivity and a lower SD values. The role of *w*-ICWC was defined by generating the additional RF field using the coupling between single-channel Tx/Rx surface coil and *w*-ICWC. The amount of inductive coupling between two conductors was measured by their mutual inductance. The *w*-ICWVC was cover more large imaging area with higher mutual inductance than *w*-ICWSC. The simulation results for the $|E|$-field distribution are shown in Fig. 3. Similar $|E|$-field distributions were observed between the only single-

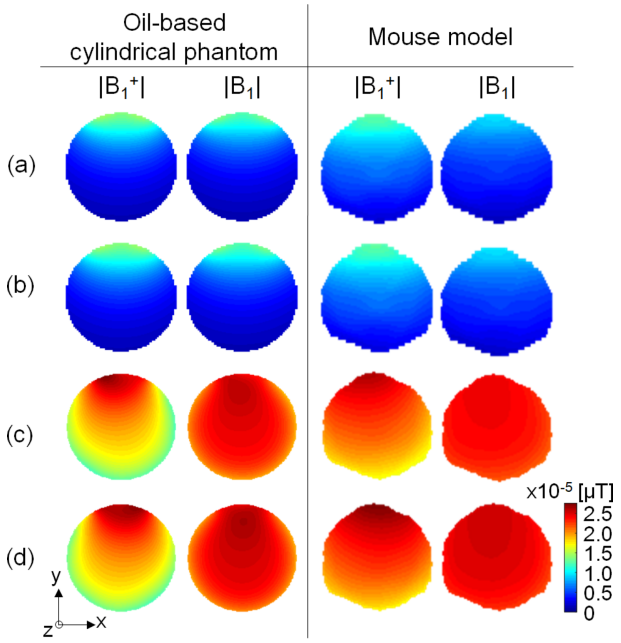

Fig. 2. (Color online) $|B_1|$-, and $|B_1^+|$-field distributions for the four coil configurations using the oil-based cylindrical phantom and mouse model: (a) single-channel Tx/Rx surface coil, (b) single-channel Tx/Rx surface coil + *w*-ICWSC, (c) single-channel Tx/Rx surface coil + *w*-ICWVC, (d) single-channel Tx/Rx surface coil + *w*-ICWSC + *w*-ICWVC.

Table 1. Measured maximum and SD values in $|B_1|$-field maps for the four coil configurations in the oil-based cylindrical phantom and the mouse model: (a) single-channel Tx/Rx surface coil, (b) single-channel Tx/Rx surface coil + w-ICWSC, (c) single-channel Tx/Rx surface coil + *w*-ICWVC, (d) single-channel Tx/Rx surface coil + *w*-ICWSC + *w*-ICWVC

	Oil-based cylindrical phantom		Mouse model	
	Maximum [μT]	SD [μT]	Maximum [μT]	SD [μT]
(a)	2.100	0.484	1.197	0.597
(b)	2.107	0.483	1.188	0.613
(c)	4.052	0.258	3.153	3.019
(d)	4.136	0.267	3.265	3.126

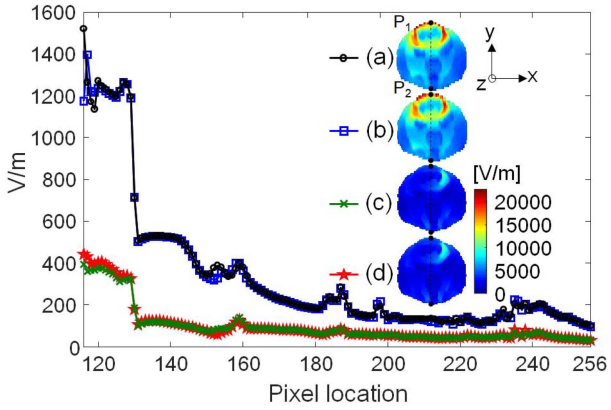

Fig. 3. (Color online) |E|-field distributions for four coil configurations using the mouse model: (a) single-channel Tx/Rx surface coil, (b) single-channel Tx/Rx surface coil + w-ICWSC, (c) single-channel Tx/Rx surface coil + *w*-ICWVC, (d) single-channel Tx/Rx surface coil + *w*-ICWSC + *w*-ICWVC.

channel Tx/Rx coil and the *w*-ICWSC, but the |E|-field intensity of the *w*-ICWVC was measured to be relatively lower than the two cases. The *w*-ICWVC coil configuration shows lower RF deposition into the subject as compared to other case. While the |E|-field distribution was concentrated between Tx/Rx coil and *w*-ICWSC, The *w*-ICWVC has the dispersed along the *w*-ICWC structure.

4. Conclusion

A single-channel Tx/Rx surface coil and a single-channel birdcage coil has become the standard coil for mouse head imaging as well as clinical MRI. Each coil was utilized individually for the target imaging region. In this study, we proposed a combination of the single-channel Tx/Rx surface coil with the *w*-ICWSC and *w*-ICWVC for mouse head imaging at 9.4-T, which was different from the existing method which employs the *w*-ICWSC or *w*-ICWVC. The study findings provide a new direction for the improvement of $|B_1|$-field sensitivity and adaptation of coil selection for small-animal MRI.

Acknowledgement

This research was supported by a grant (HO16C0004) from Osong innovation center funded by the ministry of health & welfare, the republic of Korea. We would like to thank ZMT for providing free license of Sim4Life used in this study.

References

[1] W. A. Edelstein, G. H. Glover, C. J. Hardy, and R. W. Redington, Magn. Reson. Med. **3**, 604 (1986).
[2] V. Hartwig, G. Giovannetti, N. Vanello, M. Lombardi, L. Landini, and S. Simi, Int. J. Environ. Res. Public Health. **6**, 1778 (2009).
[3] P. A. Bottomley and E. R. Andrew, Phys. Med. Biol. **23**, 630 (1978).
[4] L. L. Arnder, M. D. Shattuck, and R. D. Black, Magn. Reson. Med. **35**, 727 (1996).
[5] R. G. Pinkerton, E. A. Barberi, and R. S. Menon, Magn. Reson. Med. **54**, 499 (2005).
[6] C. E. Hayes and L. Axel, Med. Phys. **12**, 604 (1985).
[7] M. D. Schnall, C. Barlow, V. H. Subramanian, and J. S. Leigh, J. Magn. Reson. **68**, 161 (1986).
[8] A. G. Webb, Concepts Magn. Reson. Part A. **38**, 148 (2011).
[9] Sim4Life by ZMT, www.zurichmedtech.com
[10] J. Wang, Q. X. Yang, X. Zhang, C. M. Collins, M. B. Smith, X. Zhu, G. Adriany, K. Ugurbil, and W. Chen, Magn. Reson. Med. **48**, 362 (2002).